Super-virtual Interferometric Diffractions as Guide Stars

Wei Dai[1], *Tong Fei*[2], *Yi Luo*[2] *and Gerard T. Schuster*[1]
[1]*King Abdullah University of Science and Technology*
[2]*Saudi Aramco*

SUMMARY

A significant problem in seismic imaging is seismically *seeing* below salt structures: large velocity contrasts and the irregular geometry of the salt-sediment interface strongly defocus both the downgoing and upgoing seismic wavefields. This can result in severely defocused migration images so as to seismically render some subsalt reserves invisible. The potential cure is a good estimate of the subsalt and salt velocity distributions, but that is also the problem: severe velocity contrasts prevent the appearance of coherent subsalt reflections in the surface records so that MVA or tomographic methods can become ineffective. We now present an interferometric method for extracting the diffraction signals that emanate from diffractors, also denoted as seismic guide stars. The signal-to-noise ratio of these interferometric diffractions is enhanced by $\sqrt{N}$, where N is the number of source points coincident with the receiver points. Thus, diffractions from subsalt guide stars can then be rendered visible and so can be used for velocity analysis, migration, and focusing of subsalt reflections. Both synthetic and field data records are used to demonstrate the benefits and limitations of this method.

INTRODUCTION

Many of the world's giant oil reservoirs discovered in the 21st century are offshore marine fields, and a significant number of them are below salt. For example, deep drilling in the Gulf of Mexico is exclusively below a large salt horizon that blankets the Gulf of Mexico beneath depths of 5 km or more. Another example is offshore Brazil where large scale imaging, drilling, and extraction of subsalt hydrocarbons are carried out. The main challenges with deep subsalt deposits are that they are difficult to identify with the seismic method, and they are extremely expensive to drill and extract. Thus, improving the accuracy of subsalt imaging with the seismic method is an important goal of many large oil companies.

A significant problem with the seismic imaging method is that subsalt reflections are severely defocused by the strong velocity contrasts and the irregular geometries of salt-sediment interfaces. Upgoing reflection energy is present in the data, but cannot be easily detected in the shot records as coherent arrivals with hyperbolic-like moveout trajectories. This means that velocity estimation methods such as traveltime tomography cannot be used and, others, such as migration velocity analysis or full-wave inversion will fail unless an accurate starting velocity model is used. Is there another means for estimating subsalt velocities when the other methods fail?

This paper proposes interferometric extraction of subsalt diffractions, with the possibility that they can also be used as migration operators or for velocity analysis. The key idea (see Figure 1) is that, similar to surface waves or refractions, 2D subsalt diffractions are associated with stationary source points all along the source line. Thus, application of interferometry can enhance the signal-to-noise ratio of this diffraction energy by $\sqrt{N}$, where N is the number of source points. This means that undetectable diffractions in the shot records can be enhanced, which can then be used to guide velocity analysis and focusing of subsalt reflections. We refer to such diffractors as guide stars because they, similar to VSP data, can be used as Green's functions to build natural migration operators (Schuster, 2002; Brandsberg-Dahl et al., 2007), or estimate migration velocity (Berkhout et al., 2001; Landa et al., 1987). Similar to guide stars used by astronomers for correcting the optical distortion of the atmosphere, diffraction based migration operators can be used to guide the proper focusing of subsalt reflection energy to their points of origin beneath the salt. Both synthetic and field data records are used to demonstrate the benefits and limitations of this method.

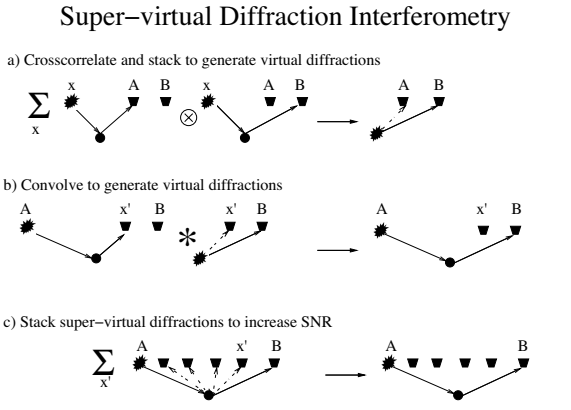

Figure 1: The steps for creating super-virtual diffraction arrivals. (a) Correlation of the recorded trace at **A** with that at **B** for a source at **x** to give the correlated trace $\phi_x(\mathbf{A},\mathbf{B},t)$ with the virtual diffraction having traveltime denoted by $\tau_{A'B}-\tau_{A'A}$. This arrival time will be the same for all source positions x, so stacking $\sum_x \phi_x(\mathbf{A},\mathbf{B},t)$ will enhance the SNR of the virtual diffraction by $\sqrt{N}$. (b) Similar to that in (a) except the virtual diffraction traces are convolved with the actual diffraction traces and stacked for different geophone positions x' to give the (c) super-virtual trace with an enhanced SNR. Here, N denotes the number of coincident source and receiver positions.

The first part of this paper presents the interferometric theory for extracting diffraction energy in seismic records. This is followed by synthetic and field data examples that show both the benefits and limitations of this method, and finally the last section presents a summary.

THEORY

We will first present the far-field reciprocity equations of correlation and convolution types, and then show how they can be used to construct super-virtual diffractions. The use of the far-field reciprocity equations of correlation and convolution types to create virtual diffractions and enhance their SNR is similar to that of Mallinson et al. (2011), except diffraction energy is enhanced rather than refraction energy. We will assume an acoustic medium with an arbitrary velocity distribution with constant density, and wideband sources with unity amplitude at each frequency.

Reciprocity Equations of Correlation Type

Assume a source at $\mathbf{x}$ in Figure 2 and receivers at $\mathbf{A}$ and $\mathbf{B}$. The reciprocity theorem of correlation type (Wapenaar and Fokkema, 2006) states that the virtual Green's function $G(\mathbf{B}|\mathbf{A})^{virt.}$ is given by the reciprocity theorem of correlation type:

$$\mathbf{B},\ \mathbf{A} \in V_0;\ \ 2iIm[G(\mathbf{B}|\mathbf{A})^{virt.}] = \int_{top} [G(\mathbf{B}|\mathbf{x})^* \frac{\partial_x G(\mathbf{A}|\mathbf{x})}{\partial n} - G(\mathbf{A}|\mathbf{x}) \frac{\partial_x G^*(\mathbf{B}|\mathbf{x})}{\partial n}] d^2x, \quad (1)$$

where $\frac{\partial_x G(\mathbf{A}|\mathbf{x})}{\partial n} = \nabla G(\mathbf{A}|\mathbf{x}) \bullet \hat{n}$ for the outward point unit normal $\hat{n}$ on the boundary. Here, Green's function solves the Helmholtz equation for an arbitrary velocity distribution with a constant density and we follow the notation from Schuster (2009). The integration path is only over the *top* path as the half-circle path is neglected by the Wapenaar anti-radiation condition.

Now we want the diffractions to be reinforced so $G(\mathbf{A}|\mathbf{B})$ is replaced by the diffraction term defined as $\mathscr{G}(\mathbf{A}|\mathbf{B})$ to give, under the far-field approximation,

$$Im[\mathscr{G}(\mathbf{B}|\mathbf{A})^{virt.}] \approx k \int_{top} \mathscr{G}(\mathbf{A}|\mathbf{x})^* \mathscr{G}(\mathbf{B}|\mathbf{x}) d^2x, \quad (2)$$

where k is the average wavenumber and $\mathscr{G}(\mathbf{B}|\mathbf{A}) = G(\mathbf{B}|\mathbf{A})^{diff.}$ represents the diffraction contribution in the Green's function for a point scatter.

This approximation is analogous to that used in model-based redatuming of reflection data to a new datum, except in model-based datuming $\mathscr{G}(\mathbf{A}|\mathbf{x})^*$ is a model-based extrapolation Green's function that only accounts for direct arrivals, and $\mathscr{G}(\mathbf{B}|\mathbf{x})$ represents the reflection data devoid of direct waves and multiples.

According to the ray diagram in Figure1(a), the correlated trace $\mathscr{F}^{-1}[\mathscr{G}(\mathbf{A}|\mathbf{x})^* \mathscr{G}(\mathbf{B}|\mathbf{x})]$ ($\mathscr{F}^{-1}$ denotes the temporal inverse Fourier transform) for a source at $\mathbf{x}$ has the same traveltime $\tau_{A'B} - \tau_{A'A}$ for any source location $\mathbf{x}$. Such source locations are considered to be at stationary points, and similar to surface wave interferometry (Xue et al., 2009) or refraction wave interferometry (Dong et al., 2006), the summation of the correlated records over source positions tend to enhance the SNR of the virtual diffraction arrival by a factor of $\sqrt{N}$. Here, N represents the number of source positions that generate the diffractions.

Reciprocity Equations of Convolution Type

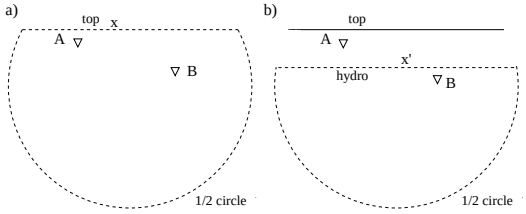

Figure 2: (a) Geometry for computing virtual Green's functions $G(\mathbf{B}|\mathbf{A})$ from the recorded data $G(\mathbf{A}|\mathbf{x})$ and $G(\mathbf{B}|\mathbf{x})$ using the reciprocity theorem of correlation type in an arbitrary acoustic medium of constant density. (b) Geometry for computing super-virtual Green's functions $G(\mathbf{B}|\mathbf{A})^{super}$ from the recorded data $G(\mathbf{A}|\mathbf{x}')$ and the virtual data $G(\mathbf{B}|\mathbf{x}')^{virt.}$ using the reciprocity theorem of convolution type.

It is assumed that the virtual data $G(\mathbf{B}|\mathbf{A})^{virt.}$ can be extrapolated to get $G(\mathbf{x}'|\mathbf{A})^{virt.}$ for $\mathbf{x}'$ along the horizontal dashed line in Figure 2(b); similarly, the field data can be extrapolated to get $G(\mathbf{x}'|\mathbf{B})$. In this case, the reciprocity theorem of convolution type (Schuster, 2009) can then be used to obtain the super-virtual data

$$G(\mathbf{B}|\mathbf{A})^{super} \approx \int_{hydro} [G(\mathbf{B}|\mathbf{x}') \frac{\partial_{\mathbf{x}'} \mathbf{G}(\mathbf{A}|\mathbf{x}')}{\partial \mathbf{n}'} - \mathbf{G}(\mathbf{A}|\mathbf{x}') \frac{\partial_{\mathbf{x}'} \mathbf{G}(\mathbf{B}|\mathbf{x}')}{\partial \mathbf{n}'}] \mathbf{d^2 x}', \quad (3)$$

where the integration is along the *hydro* dashed line in Figure 2(b). Under the far-field approximation and setting $G(\mathbf{A}|\mathbf{x}') \rightarrow \mathscr{G}(\mathbf{A}|\mathbf{x}')$ and $G(\mathbf{B}|\mathbf{x}') \rightarrow \mathscr{G}(\mathbf{B}|\mathbf{x}')^{\mathbf{virt.}}$, we get

$$\mathscr{G}(\mathbf{B}|\mathbf{A})^{super} \approx 2ik \int_{hydro} \mathscr{G}(\mathbf{B}|\mathbf{x}')^{virt.} \mathscr{G}(\mathbf{A}|\mathbf{x}') d^2x', \quad (4)$$

where $\mathscr{G}(\mathbf{B}|\mathbf{A})^{super}$ represents the super-virtual data obtained by convolving the recorded data $\mathscr{F}^{-1}[\mathscr{G}(\mathbf{A}|\mathbf{x}')]$ with the virtual data $\mathscr{F}^{-1}[\mathscr{G}(\mathbf{B}|\mathbf{x}')^{virt.}]$. Here, the SNR of the reconstructed diffraction arrival is enhanced by the factor $\sqrt{N}$. However, practical considerations such as artifacts associated with limited recording apertures, discrete source and receiver sampling, windowing of the diffracted waves, and the far-field approximation will likely prevent the attainment of this ideal enhancement.

In the next section, we will use the example of diffractions that have been windowed from the original data so that $G(\mathbf{A}|\mathbf{x}) \approx G(\mathbf{A}|\mathbf{x})^{diff.}$.

SYNTHETIC DATA EXAMPLE

To demonstrate the effectiveness of the proposed method, super-virtual diffraction arrivals are extracted from synthetic shot gathers computed with a 2-4 FD forward modeling code for part of the BP2004 model. Three diffractors are placed under the salt body as shown in Figure 3. The goal is to extract the diffraction arrivals associated with these diffractors. Four hundred shot gathers are generated with a 20-Hz Ricker wavelet

and a 20 m interval. All the shots are recorded by the same 800 receivers with a 10 m interval. The sources and receivers are placed at the depth of 10 m, and the free surface condition is not implemented. A common shot gather is shown in Figure 4(a). The diffractions associated with the point diffractor on the right of the salt body are indicated with dashed red lines. These diffractions are identified by comparison against the predicted diffraction traveltimes for that diffractor, and Figure 4(b) shows these time-windowed diffractions. In order to eliminate other coherent events in the time window, a median filter is applied to these data in Figure 4(b) along the diffraction moveout curve (Moser et al., 1999) and the result is shown in Figure 4(c), where the diffractions are enhanced. However, Figure 4(c) contains strong artifacts from other coherent signals, because within the time window in Figure 4(b) the amplitudes of the direct waves are an order of magnitude greater than the amplitudes of the diffraction events. Figure 4(d) shows the super-virtual diffraction with improved SNR compared to the result after median filtering in Figure 4(c).

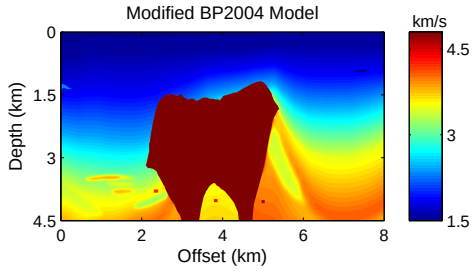

Figure 3: Part of the BP2004 velocity model with three diffractors below the salt body.

Another synthetic example is shown to illustrate that the super-virtual diffraction can be used to estimate the source and receiver statics. Synthetic data are generated with the same acquisition geometry as in the previous example for the Figure 5 velocity model. Random noise and random statics are added in the common shot gather in Figure 6(a), where the red lines outline the diffraction arrivals for the left most diffractor. In Figure 6(b), the diffraction energy is almost invisible because of the random noise, so that median filtering fails when it is applied along the predicted hyperbolic moveout (Figure 6(c)). Since the diffraction arrivals are temporally isolated from other events, the super-virtual diffraction is obtained without median filtering and shown in Figure 6(d). The actual moveout curve of the diffraction is preserved and plotted as the blue line in Figure 7. In this figure, the red line indicates the predicted arrival time of the diffraction without considering the source and receiver statics. The source and receivers statics can now be estimated from the difference between the blue and red lines or by a phase closure principle (Sheng et al., 2005). In addition, the moveout curve can be used to represent the Green's function $G(\mathbf{B}|\mathbf{x}_o)$ for a point source at $\mathbf{x}_o$, which can be used as the natural migration operator $G(\mathbf{B}|\mathbf{x}_o)^* G(\mathbf{A}|\mathbf{x}_o)^*$ (Schuster, 2002).

FIELD DATA EXAMPLE

In this section, the proposed method is applied to the Friendswood cross-well data to extract super-virtual diffraction arrivals. This data set was collected at Exxon's test site located near Friendswood, Texas. The source and receiver intervals are both 3.05 m and the distance between the two wells is 182.9 m. There are 98 shot gathers with 96 traces each in this data set. Figure 8(a) shows a raw common shot gather and the target diffraction is outlined with 2 red lines. A zoom view of the diffraction is shown in Figure 8(b). In this example, the moveout of the diffraction is manually picked for the purpose of median filtering and Figure 8(c) shows the result after applying a median filter along the moveout curve. It is clear that the coherent noise is effectively removed by median filtering. To further improve the result, the super-virtual diffraction method is applied to the median-filtered events and the result is shown in Figure 8(d), which is of much higher SNR compared to Figure 8(c).

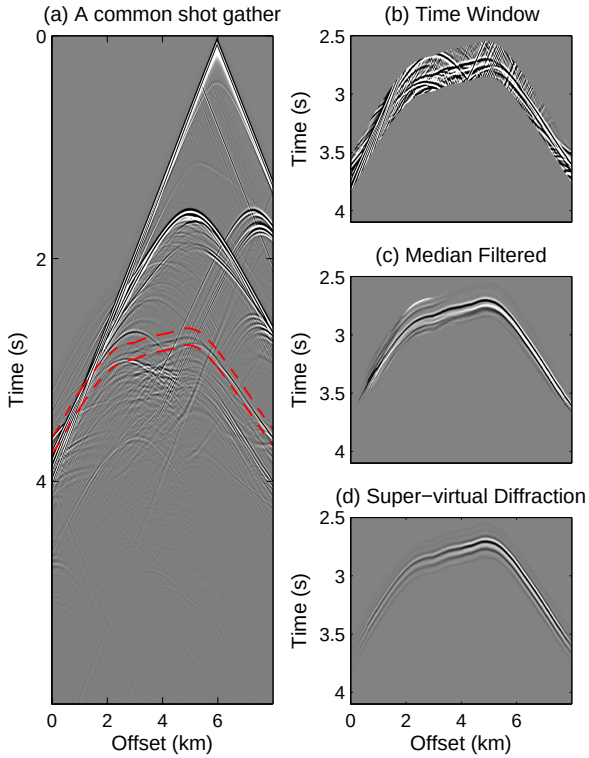

Figure 4: Synthetic data results for part of the BP2004 model. (a) A common shot gather with a source at offset 6 km. Red lines indicate the time window and the moveout of the diffraction event. (b) The diffraction event within a small time window. (c) The result after median filtering and (d) after processing the median filtered data to get the super-virtual diffraction.

CONCLUSION

We presented the general theory of super-virtual diffraction interferometry where the signal-to-noise ratio (SNR) of diffrac-

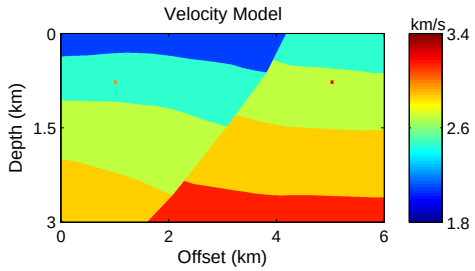

Figure 5: Velocity model with a fault and two diffractors.

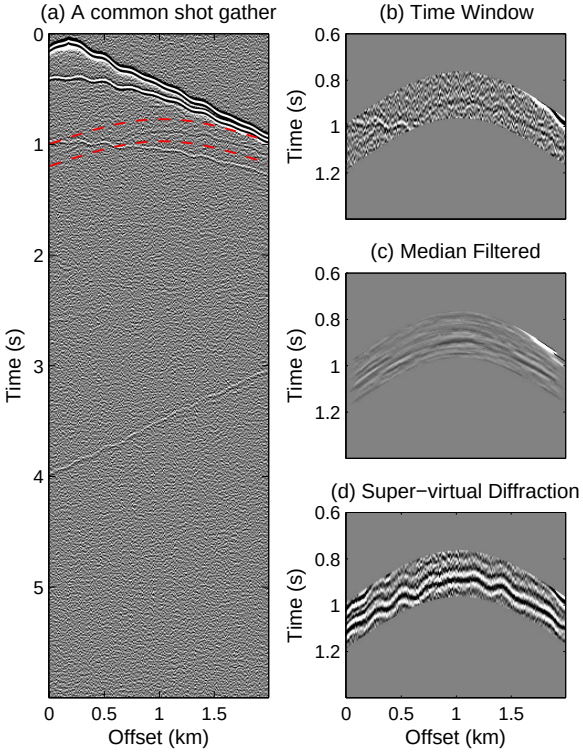

Figure 6: Synthetic data results for the fault model. (a) A common shot gather with a source at offset 36 m. Red lines indicate the time window of the diffraction event. (b) The diffraction event within a small time window. (c) The result after median filtering and (d) after processing the raw data to get the super-virtual diffraction.

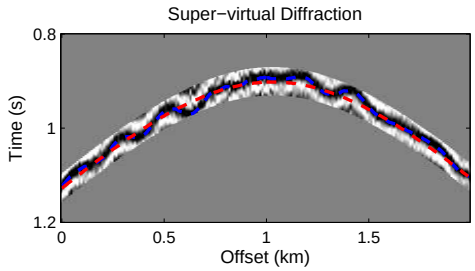

Figure 7: The super-virtual diffraction. In this figure, the red line indicates the predicted diffraction arrival times and the blue line indicates the picked arrival times.

tion arrivals can be theoretically increased by the factor $\sqrt{N}$, where N is the number of receiver and source positions associated with the recording of the diffractions. There are two steps to this methodology: correlation and summation of the data to generate traces with virtual diffraction arrivals, followed by the convolution and stacking of the data with the virtual traces to create super-virtual diffractions. This method is valid for any medium that generates diffraction arrivals due to isolated subwavelength scatterers. There are at least three benefits with this methodology: 1). the diffraction arrivals can be used as migration operators (Schuster, 2002; Brandsberg-Dahl et al., 2007; Sinha et al., 2009); 2). the diffraction arrivals can be used for estimating source and receiver statics; 3). estimation of velocities by traveltime tomography or MVA.

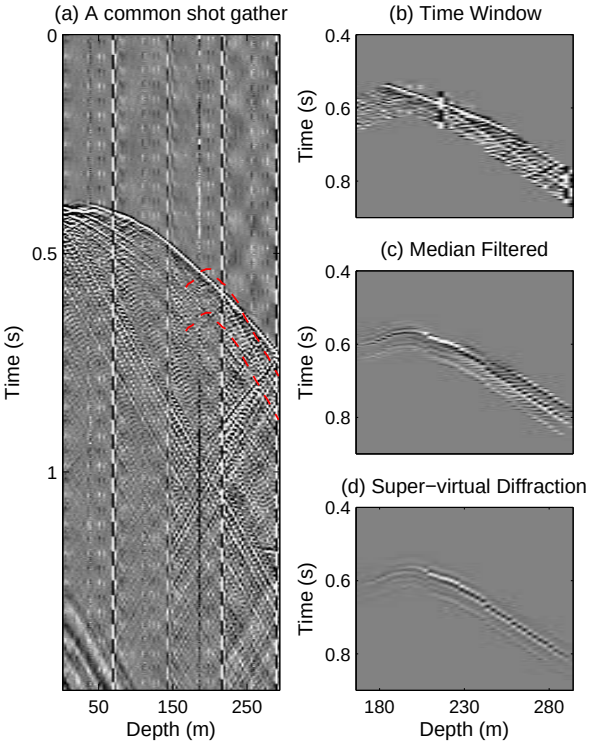

Figure 8: Friendswood cross-well data example. (a) A common shot gather with a source at depth of 36.6 m. Red lines indicate the time window and the moveout of the diffraction event. (b) The diffraction event within a small time window. (c) The result after median filtering and (d) the super-virtual diffraction.

The problem with this method is that there will be artifacts associated with coherent events and quality degradation due to a limited recording aperture and a coarse spacing of the source and receivers.

ACKNOWLEDGEMENTS

We thank the sponsors of the CSIM for their financial support and thank Saudi Aramco for supporting to Gerard T. Schuster during his sabbatical in 2007.

EDITED REFERENCES

Note: This reference list is a copy-edited version of the reference list submitted by the author. Reference lists for the 2011 SEG Technical Program Expanded Abstracts have been copy edited so that references provided with the online metadata for each paper will achieve a high degree of linking to cited sources that appear on the Web.

REFERENCES

Berkhout, A. J., L. Ongkiehong, A. W. F. Volker, and G. Blacquiere, 2001, Comprehensive assessment of seismic acquisition geometries by focal beams — Part I: Theoretical considerations: Geophysics, **66**, 911–917, doi:10.1190/1.1444981.

Brandsberg-Dahl, S., B. Hornby, and X. Xiao, 2007, Migration of surface seismic data with VSP Green's functions: The Leading Edge, **26**, 778–780, doi:10.1190/1.2748496.

Dong, S., J. Sheng, and J. T. Schuster, 2006, Theory and practice of refraction interferometry: 76th Annual International Meeting, SEG, Expanded Abstracts, **25**, 3021–3025.

Landa, E., V. Shtivelman, and B. Gelchinsky, 1987, A method for detection of difracted waves on common-offset sections: Geophysical Prospecting, **35**, no. 4, 359–373, doi:10.1111/j.1365-2478.1987.tb00823.x.

Mallinson, I., P. Bharadwaj, G. T. Schuster, and H. Jakubowicz, 2011, Enhanced refractor imaging by super-virtual inteferometry: The Leading Edge, **30**, 546–550.

Moser, T. J., E. Landa, and S. A. Petersen, 1999, Velocity model based diffraction filtering: 69th Annual International Meeting, SEG, Expanded Abstracts, **18**, 1174–1177.

Schuster, G. T., 2002, Reverse-time migration = Generalized diffraction stack migration: 72nd Annual International Meeting, SEG, Expanded Abstracts, **21**, 1280–1283.

———, 2009, Seismic interferometry: Cambridge University Press.

Sheng, J., J. Yu, and G. T. Schuster, 2005, Tomostatics and closure phase residual statics applied to Saudi Aramco land data: 75th Annual International Meeting, SEG, Expanded Abstracts, **24**, 2229–2232.

Sinha, S., B. Hornby, and R. Ramkhelawan, 2009, 3D depth imaging of surface seismic using VSP measured Green's function: 79th Annual International Meeting, SEG, Expanded Abstracts, **28**, 4125–4128.

Wapenaar, K., and J. Fokkema, 2006, Green's function representations for seismic interferometry: Geophysics, **71**, no. 4, SI33–SI46, doi:10.1190/1.2213955.

Xue, Y., S. Dong, and G. T. Schuster, 2009, Interferometric prediction and subtraction of surface waves with a nonlinear local filter: Geophysics, **74**, no. 1, SI1–SI8, doi:10.1190/1.3008543.